Megathrust Locking and Viscous Mantle Flow Induce Continental Shortening in Central Andes

Fuqiang Shi, Shaoyang Li & Marcos Moreno

Pure and Applied Geophysics
pageoph

ISSN 0033-4553

Pure Appl. Geophys.
DOI 10.1007/s00024-019-02403-0

Springer

Pure Appl. Geophys.

https://doi.org/10.1007/s00024-019-02403-0

Pure and Applied Geophysics

Megathrust Locking and Viscous Mantle Flow Induce Continental Shortening in Central Andes

Fuqiang Shi,[1] Shaoyang Li,[2] and Marcos Moreno[3]

Abstract—Crustal faults at subduction zones show evidence of activity over geological time, but at the scale of earthquake cycle the mechanical behavior of these faults is not fully understood. Here we construct 2-D viscoelastic models constrained by both horizontal and vertical GPS-derived interseismic velocities to investigate the contribution and interrelation between subduction zone locking, viscous mantle flow, and upper plate faulting on surface deformation in Central Andes. Main pattern of horizontal velocities can be explained by a combination of locking degree and viscous flow, whereas vertical signal is found essential for estimating the locking depth. A sharp deformation gradient near the major back-arc fault suggests an active interseismic shorting across this structure. We further conduct mechanical viscoelastic models with a frictional back-arc fault to analyze its displacement and activation conditions. Our results suggest that the back-arc fault is creeping at $\sim$ 3 mm/year and its motion is mainly driven by the interseismic viscous mantle flow, which spreads plate tectonic stresses broadly across the continent. Moreover, the frictional strength of the back-arc fault must be remarkably weak and its mechanics re-distributes the interseismic deformation and shortens the continental plate in Central Andes. Geological estimates suggest that the long-term shortening rate at the back-arc fault is $\sim$ 10 mm/year, suggesting that this structure can accumulate $\sim$ 7 mm/year of slip deficit, confirming the seismic potential of this structure.

Keywords: Central Andes, interseismic deformation, viscoelastic relaxation, mechanical modeling, back-arc shortening, GPS, finite element models, subduction zone.

1. Introduction

Active deformation of major continental faults at convergent margins provides key insights into Earth dynamics and evolution (e.g., earthquake distribution, strain partitioning, and mountain building). The kinematics of these faults are commonly modeled as rigid microplate motions under the assumption of purely elastic Earth's blocks (e.g., Bevis et al. 2001; Brooks et al. 2003; Chlieh et al. 2011; Loveless and Meade 2010; McCaffrey et al. 2000a; b; Wallace et al. 2004). Mechanically, these modeled continental-fault motions are unrelated to subduction faulting processes, which could drive significant short- and long-term viscoelastic relaxations in the asthenosphere through the megathrust earthquake cycles (e.g., Cohen 1984; Matsu'ura and Sato 1989; Savage 1983; Wang et al. 2012). More specifically, during the interseismic period, stresses slowly built up due to megathrust fault locking are relaxed concurrently resulting wide-spread viscoelastic deformation across the continental faults till very far field at subduction zones (Wang et al. 2012; Li et al. 2015).

The Central Andes is the highest and widest part of the Andean mountain belt in Southern American plate (insert plot of Fig. 1a), which is believed to be caused by rapid crustal shortening due to the subduction of Nazca plate since last $\sim$ 25 Ma (e.g., Allmendinger et al. 1997; Isacks 1988). This subduction zone has been long identified as a mature seismic gap since last great megathrust event in 1877 (Mw $\sim$ 8.8, Comte and Pardo 1991). Present-day Global Positioning System (GPS) measurements clearly show that the horizontal interseismic deformation spreads extensively more than 800 km from the trench into the back-arc region (Brooks et al. 2011) (Fig. 1a). Such slowly decaying, long-wavelength deformation pattern ($>$ 700 km) could be successfully explained by the subduction fault locking based on a viscoelastic Earth model (Li et al.

Electronic supplementary material The online version of this article (https://doi.org/10.1007/s00024-019-02403-0) contains supplementary material, which is available to authorized users.

[1] Shaanxi Earthquake Agency, Xi'an, China.
[2] Earthquake Research Institute, University of Tokyo, Tokyo, Japan. E-mail: shaoyangli@eri.u-tokyo.ac.jp
[3] Departamento de Geofísica, Facultad de Ciencias Físicas y Matemáticas, Universidad de Concepción, Concepción, Chile.

Published online: 08 January 2020

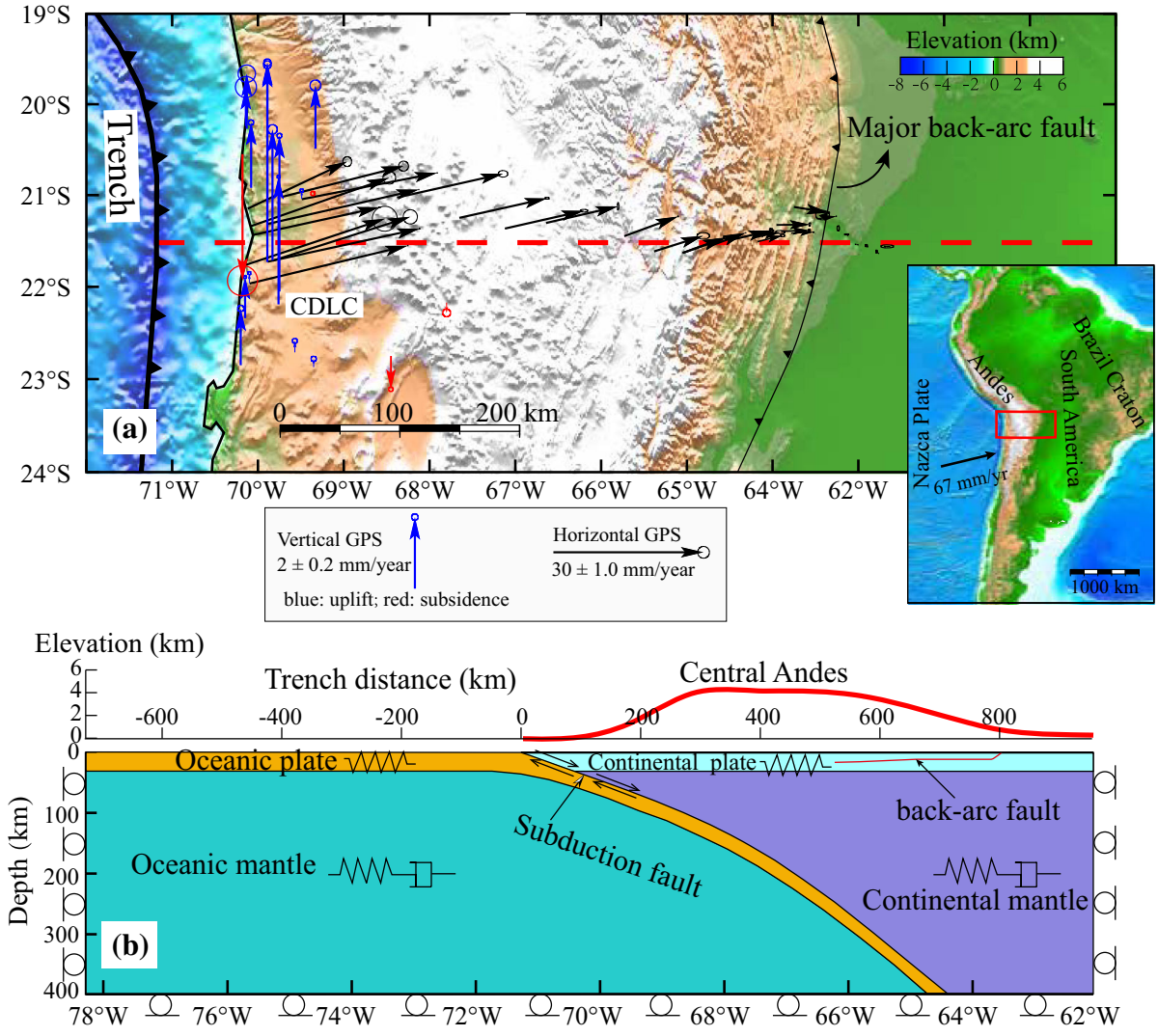

Figure 1

a Tectonic settings and the GPS-derived horizontal and vertical velocities in Central Andes. The red rectangle in the insert (lower right) shows the location of study area in Nazca-South America subduction zone. The station CDLC is taken as an example of GPS time series analysis shown in supporting information. **b** Model setups of the viscoelastic models. The oceanic and continental plates are assumed as purely elastic; the oceanic and continental mantle are assumed to be viscoelastic and simulated with linear Maxwell rheology. The symbols along the eastern, western, and bottom boundaries indicate that displacement is not allowed perpendicular to, but is allowed parallel to the boundary. The red curve above the model geometry is the smoothed elevation along the red dashed line in Fig. 1a

2015). Further inland, a decadal GPS profile (at ~ 21.5° S) unambiguously shows a sharp velocity gradient (SVG) within a distance shorter than 100 km across a major back-arc fault (Kendrick et al. 2001; Brooks et al. 2011) (Fig. 1a). Such gradient was attributed to the full locking of a sub-horizontal back-arc fault right beneath the area of SVG based on Euler vectors and kinematic inversions of elastic half-space models (Bevis et al. 2001; Brooks et al. 2011; Weiss et al. 2016). However, these models are mechanically independent to subduction processes and explain all the nearby velocities by only the dislocation of the back-arc fault and rotation of rigid blocks. Therefore, they have difficulties to explain whether and how the back-arc fault is dynamically driven or influenced by the subduction processes,

especially the far-field-approaching interseismic viscoelastic relaxation in mantle.

In this study, we first perform a suite of 2-D forward viscoelastic models (Fig. 1b) to explore the first-order deformation signals due to megathrust locking and viscoelastic relaxation of the continental mantle. By examining the model fitting of both horizontal and vertical deformation rates, we gain insights on the effects of the two processes on both horizontal and vertical deformation directions and better constrain their reasonable parameter spaces. Then, we further investigate the feedback between fore-arc deformation and major back-arc faulting by performing mechanical viscoelastic models, in which a frictional back-arc fault is included. We analyze the activation conditions (i.e., megathrust locking depth, continental mantle viscosity, and effective friction coefficient of the back-arc fault) for the back-arc fault that can explain the observed SVG. Based on the fitting of all the GPS-derived velocities, we propose our optimal mechanical model. Finally, we discuss the implications of plate tectonics and the present-day crust shortening in Central Andes.

2. GPS-derived Velocities

There are two published updated GPS-derived horizontal velocity profiles in Central Andes at ∼ 21.5° S and ∼ 19.5° S (Brooks et al. 2011; Weiss et al. 2016), respectively. In this study, we choose to model the profile at ∼ 21.5° S over the other profile because this profile has been maintained over a longer survey time [i.e., a decade on average from 1990s to 2014 (Weiss et al. 2016)]. The coseismic and postseismic signals of some previous large earthquakes (e.g., the 2007 Mw 7.8 Tocopilla earthquake) have been removed from these velocities (Weiss et al. 2016). Respecting to a fixed South American craton reference frame (Weiss et al. 2016), this profile features gentle decrease of velocity over a broad region (> 700 km), i.e., from ∼ 30 mm/year at the coastline to ∼ 5 mm/year in the back-arc region (Figs. 1a, and 2d). Near the major back-arc fault, the velocity decreases sharply from ∼ 5 to 0 mm/year over a relatively narrow region (< 100 km, between 63 and 64° W). This decrease (∼ 5 mm/year) is used roughly as the SVG observed in GPS data.

In order to better constrain the reasonable locking depth and continental mantle viscosity (Sect. 4.1), we additionally analyze daily time series of continuous GPS data from Nevada Geodetic Laboratory (http://geodesy.unr.edu/index.php) to retrieve the vertical interseismic velocities. Details of GPS time series analysis are described in Text S1 with an example of station CDLC shown as Figure S1 in the supporting information. Due to the limitation of available stations, vertical velocities concentrate only in the fore-arc area (< 400 km trench distance, Figs. 1a and 2e) but they clearly exhibit an uplift signal (∼ 5 mm/year) near the coast with almost no displacement signal in the western cordillera.

3. Modeling Strategy

Our models are constructed using the open source finite element code *PyLith* (Aagaard et al. 2013). The 2-D model geometry (Fig. 1b) is extracted from the 3-D Peru-Northern Chile model of Li et al. (2015) as a profile at 21.5° S (comparable to the GPS-derived velocities) and the geometry of the major back-arc fault (Fig. 1b) is adapted from Brooks et al. (2011), which was constructed based on seismic reflection studies (Moretti, et al. 1996; Uba et al. 2009). We implement the back-slip model (Savage 1983) and specify material properties and boundary conditions (sketched in Fig. 1b) following the modeling strategy of Li et al. (2015). In our interseismic viscoelastic models, we ignore the effects of postseismic relaxation of previous great event because its effects would vanish soon in a few decades for the typical earthquake size in North Chile (Sun et al. 2018). Therefore, the viscoelastic relaxation effects considered in this study are from the re-locking of plate-interface since the last event in 1877 (Comte and Pardo 1991). More details of model setups are provided as Text S2 in the supporting information.

In this study, we first perform viscoelastic forward models without the major back-arc fault in a grid-searching fashion by varying the values of continental mantle viscosity and subduction locking depth. This model is hereafter called as the viscoelastic kinematic

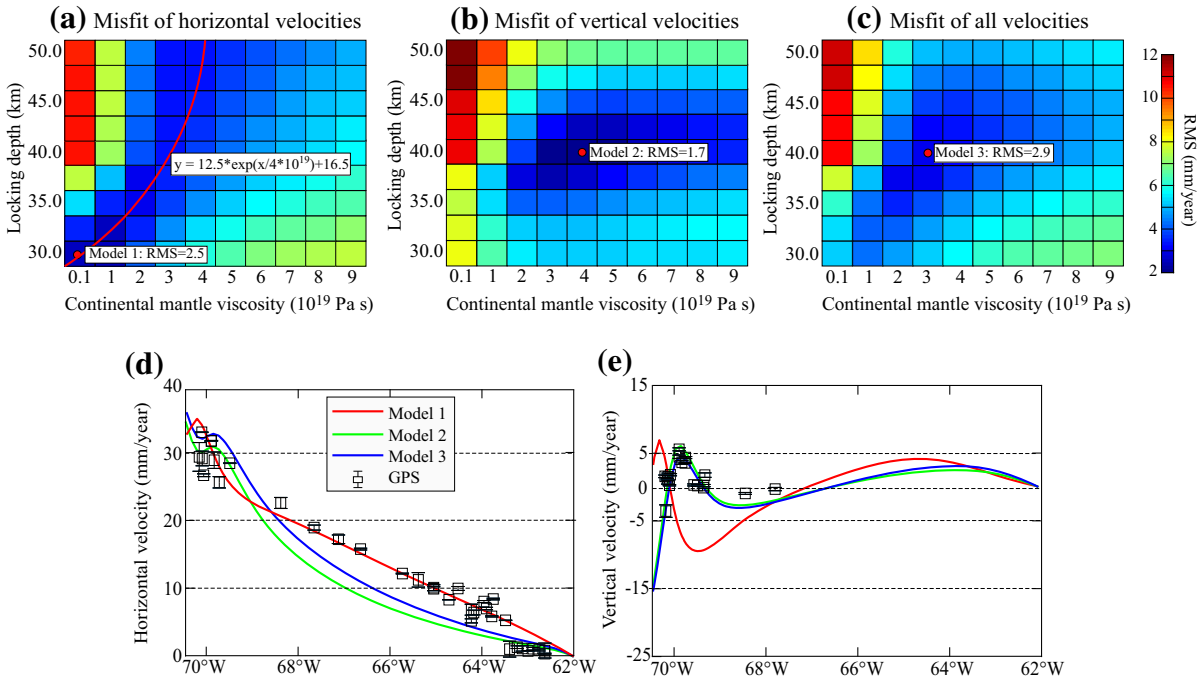

Figure 2

a–c Show the root mean square (RMS) misfit of viscoelastic kinematic models by considering horizontal, vertical, and both horizontal and vertical velocities, respectively. The red dot denotes the best model in each panel. The red curve in Fig. 2a marks the trade-off between continental mantle viscosity and locking depth. The RMS values of Fig. 2c are calculated with equal weights for horizontal and vertical velocities. **d** and **e** Show the data fittings from the three best models in horizontal and vertical directions, respectively. The GPS-derived velocities are plotted with 1σ uncertainty

model. By doing so, we are able to constrain the key parameters that control the first order interseismic surface deformation. In order to simplify the problem, we use only one free parameter (namely the locking depth in this study) to characterize the locking state of the megathrust interface. This parameter is defined as a full locking depth with a transition zone as the function provided in Wang et al. (2003) (Figure S2).

As a significant step forward, we further include a frictional back-arc fault (Fig. 1b) in the viscoelastic model and impose the Coulomb failure criterion on the fault interface (Jaeger and Cook 1979): $\Gamma = \mu'\sigma + c$, where Γ is the absolute shear strength resolved onto the fault, μ' is the effective friction coefficient, σ is the fault normal stress, and c is the fault cohesion, which is ignored in the simulations for simplicity. This model is hereafter called as the viscoelastic mechanical model. We assume that the modeled system is in lithostatic equilibrium and the normal stress along the fault equals the force due to the gravity of the overlying rock column. The frictional fault starts to creep when the accumulated shear stress is larger than Γ. In order to quantitatively investigate the conditions for the activation of the back-arc fault, we vary the values of the subduction locking depth, the mantle viscosity, and μ' of the back-arc fault. The model performances are evaluated on predicting the SVG (calculated as the horizontal velocity difference on the two sides of fault tip on surface) in the narrow zone.

In the following section of the modeling results, we will demonstrate a clear trade-off between the modeled continental mantle viscosity and megathrust locking depth with only horizontal velocities. This ambiguity could be largely solved by considering the vertical velocities. More interestingly, the back-arc fault is activated only with the mantle flow of the viscoelastic Earth model and a remarkably-weak frictional strength of the fault.

4. Modeling Results

4.1. Trade-off of Continental Mantle Viscosity and Subduction Locking Depth

With the simple viscoelastic kinematic models without the back-arc fault, we systematically explore the two parameters in physically reasonable ranges in North Chile, i.e., the continental mantle viscosity from 10^{18} to 10^{20} Pa s (Wang et al. 2012) and the locking depth from 30 to 70 km (Comte et al. 1994). In order to show separately the effects of each parameter on both horizontal and vertical deformation rates, we fix one parameter and vary the other one (Figure S3). The results show that decreasing the value of continental mantle viscosity and increasing the locking depth both produce horizontal deformation spreading further into the far field in a similar fashion (Figure S3a and S3c). In contrast, decreasing the continental mantle viscosity only reduces the magnitude of vertical deformation rate but do not shift the location (i.e., the distance to the trench) of uplift signal (Figure S3b), while increasing the locking depth moves the uplift signal moving away from the trench (Figure S3d).

Most of the simulated models are summarized in terms of the root mean square (RMS) misfit of the GPS velocities (Fig. 2a–c). The results show an inherent trade-off between continental mantle viscosity and locking depth to fit the horizontal interseismic velocities with the viscoelastic Earth models (highlighted as a red curve in Fig. 2a), i.e., models with deeper locking depths and higher continental mantle viscosities and those with shallower locking depths and lower continental mantle viscosities fit the horizontal velocities equally well. Though a wide range of the continental mantle viscosity ($2–9 \times 10^{19}$ Pa s) provides reasonable model fit to the vertical velocities, the locking depth can be well constrained by these velocities within the interval of 35 to 45 km (blueish area of Fig. 2b). The optimal forward model with a locking depth of 40 km and continental mantle viscosity of 3×10^{19} Pa s (Fig. 2c) provides reasonable fitting of both the long wavelength horizontal velocities and the vertical uplifting velocities in the near field (Fig. 2c–e). However, the models presented in this subsection leave the horizontal SVG unexplained in the far field, requiring further investigations of the back-arc fault motion as described in the following subsection.

4.2. Mechanical Conditions for the Activation of the Major Back-arc Fault

First of all, we test whether a deep locking depth of megathrust could reproduce the SVG in the similar order of GPS measurements ($\sim$ 5 mm/year) in a purely elastic Earth model. Our results show that the back-arc fault is fully locked with a reasonable megathrust locking depth (30–40 km) and creeps at negligible rate even with unphysically deep megathrust locking depth ($>$ 70 km) that produce significantly smaller SVG ($\sim$ 0.1 mm/year) than the measurements (Fig. 3). It thus indicates that the elastic stress from the megathrust locking is too small to drive the movement on the back-arc fault.

Therefore, we further study the range of modeling parameters (i.e., the megathrust locking depth, continental mantle viscosity, and the effective friction coefficient of the major back-arc fault) in a viscoelastic Earth model that might successfully predict the SVG near the major back-arc fault. In order to illustrate the effects of each parameter on the activation of the back-arc fault (quantified with the magnitude of modelled SVG as labeled in Fig. 4a), we vary the value of one parameter and keep the

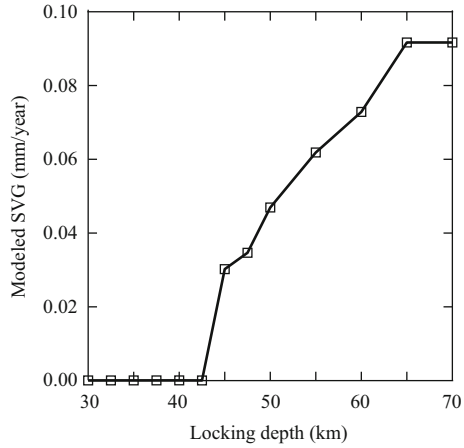

Figure 3
The modeled SVG of the back-arc fault with different locking depths in elastic Earth models. The μ' of the back-arc fault is assumed to be 0.01

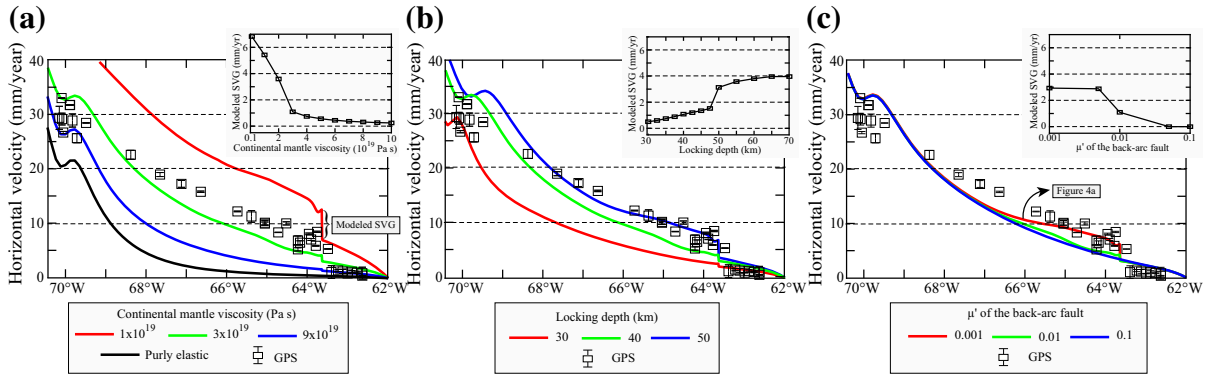

Figure 4

Effects of continental mantle viscosity, subduction locking depth, and μ' of the back-arc fault on modeling the sharp velocity gradient (SVG). **a** The continental mantle viscosity is varied with the μ' of back-arc fault and the locking depth fixed as 0.01 and 40 km, respectively. **b** The locking depth is varied with the μ' of back-arc fault and the continental mantle viscosity fixed as 0.01 and 3×10^{19} Pa s, respectively. **c** The μ' of back-arc fault is varied with the locking depth and the continental mantle viscosity fixed as 40 km and 3×10^{19} Pa s, respectively. The inset plots in the upper right of each panel show the modeled SVG as a function of each explored parameter. The black squares are GPS-derived velocities. The green curves in (a–c) are from the same model (the μ' of back-arc fault, the locking depth, and the continental mantle viscosity are 0.01, 40 km, and 3×10^{19} Pa s, respectively)

other two parameters constant. Here we take the optimal values of locking depth and continental mantle viscosity constrained from the models in the above subsection (i.e., 40 km of locking depth and 3×10^{19} Pa s of the continental mantle viscosity) as typical examples. The results show that the back-arc fault is only active with a viscoelastic mantle and the elastic model (i.e. the oceanic and continental mantle are assumed to be purely elastic similar to the elastic half-space models) predicts almost no surface deformation near the back-arc fault and no additional motion of the fault (Fig. 4a). We test unphysically deep locking depths with remarkably small μ' of the back-arc fault for elastic models and still find negligible activation of the back-arc fault (e.g., the modeled SVG is < 0.1 mm/year when the full locking depth is assumed as 70 km and the μ' is assumed as 0.01, Fig. 3). The modeled SVG decreases rapidly with the higher viscosity of continental mantle forming a "L" sharp curve (insert plot of Fig. 4a). Given a viscoelastic mantle, deeper locking depth also results larger SVG (Fig. 4b, the continental mantle viscosity is fixed as 3×10^{19} Pa s), but increasing the locking depth slowly enlarges the modeled SVG forming a "S" sharp curve (insert plot of Fig. 4b). With constant values of continental mantle viscosity and locking depth, varying the μ' impacts the deformation rates locally above the fault (Fig. 4c). Interestingly, the back-arc fault has to be remarkably weak in terms of μ' (< 0.1) to be activated by the subduction locking and viscoelastic relaxation of the mantle (insert plot of Fig. 4c). All the model results in term of modeled SVG are additionally summarized in Figure S4.

In summary, the back-arc fault is inactive with the assumption of purely elastic Earth but active with the viscoelastic mantle flow during the interseismic period consistent with the GPS observations. The continental mantle viscosity should be relatively low ($< 3 \times 10^{19}$ Pa s, which is consistent with the value used globally in Wang et al. 2012) to reproduce large enough SVG (> 4 mm/year, Figure S4). With the mantle viscoelastic relaxation, the locking depth has certain impact on modeled SVG but not as significant as the continental mantle viscosity. Moreover, the back-arc fault is activated only with remarkably low μ' (< 0.1, Figure S4).

Based on the model fitting of the wholesale horizontal (including the gentle decrease of velocities over the broad region and the SVG in the narrow zone) and the vertical (in the forearc region) GPS-derived velocities (Fig. 5), we propose our optimal mechanical model in this study (Fig. 6). The performance of the mechanical models in terms of fitting

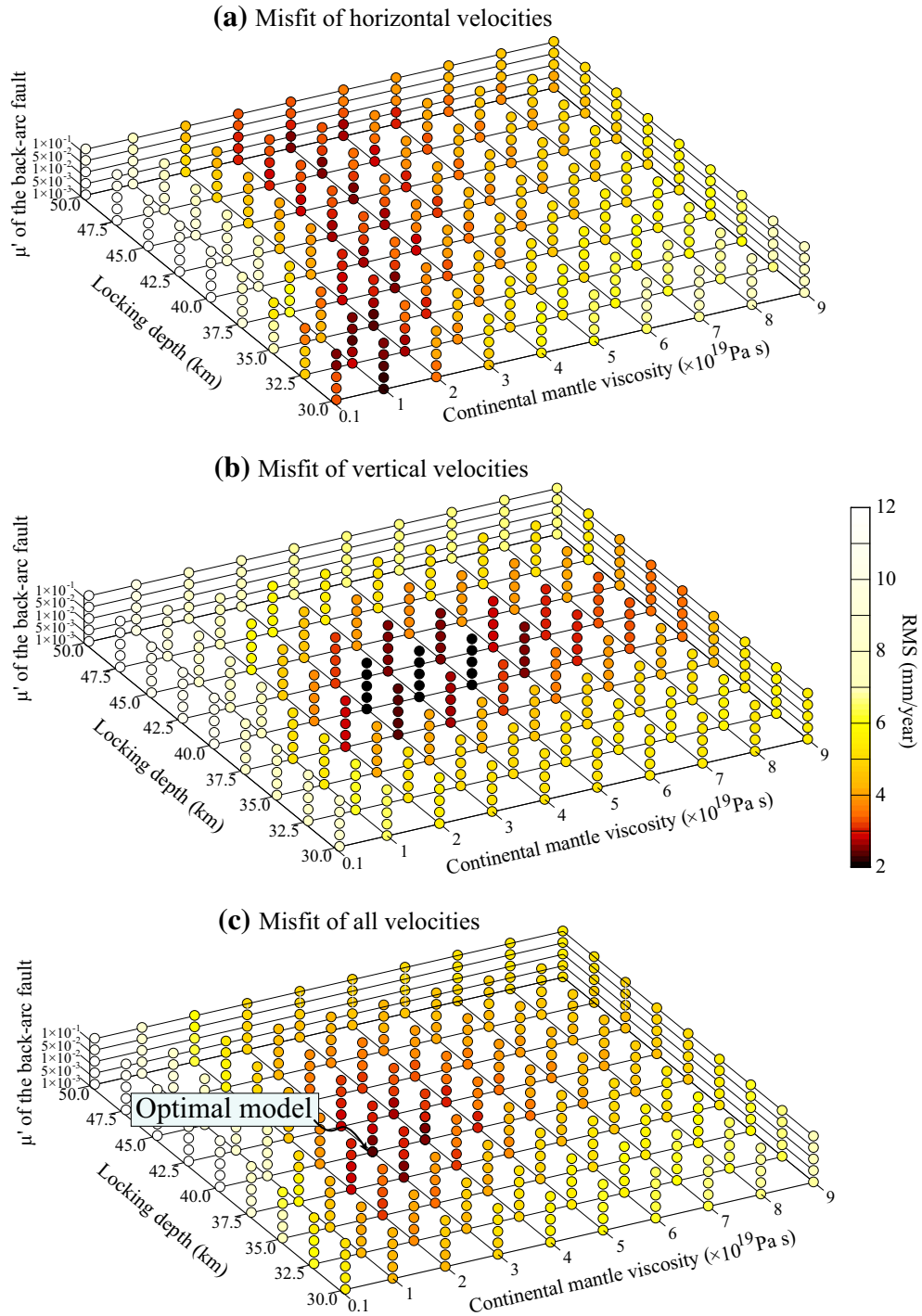

Figure 5

The root mean square (RMS) misfit of the viscoelastic mechanical models by considering **a** horizontal, **b** vertical, and **c** both horizontal and vertical GPS-derived velocities, respectively. The RMS misfit in the vertical axis decreases because of including a weak back-arc fault in the mechanical models

GPS-derived velocities is similar to that of the kinematic models (Fig. 2a–c), but the RMS misfit further decreases with a weak frictional back-arc fault (Fig. 5).

5. Discussion

Our results confirm that the interseismic viscoelastic relaxation due to the megathrust locking spreads the surface deformation across a broad region into the far field (Wang et al. 2012; Li et al. 2015). Previous studies have demonstrated that interpreting such long wavelength horizontal deformation at subduction zones with elastic models would systematically overestimate the locking depth or/and underestimate the deformation rates in the far field (e.g., Li et al. 2015, 2018b). However, most of the interseismic locking studies, assuming either elastic or viscoelastic Earth, are only considering horizontal velocities to constrain the locking state in subduction zones. In this study, we find that there is an inherent trade-off between the megathrust locking depth and the continental mantle viscosity if only using the horizontal velocities (Fig. 2a). Though vertical signal has typically much smaller magnitude than horizontal signal (e.g., the vertical signal is in between -5 and 5 mm/year and horizontal is in 0 to 35 mm/year in Central Andes case), it is particularly useful to diagnose the locking depth (Fig. 2b). Therefore, it is significantly important to measure the high quality vertical deformation (e.g., Burgette et al. 2009) and to consider both horizontal and vertical signals in the future studies of interseismic locking state in subduction zones.

In this study, we purposely simplify the structure of lithosphere-asthenosphere system beneath the Andes as two homogeneous layers with an elastic slab (Fig. 1b) and focus on the first-order interseismic deformation mechanisms (i.e., megathrust locking and mantle viscoelastic relaxation, Wang et al. 2012) to understand their influences on the activation of the back-arc fault. Weak lower crust (e.g., Pope and Willett 1998; Hyndman 2017), depth-dependent mantle viscosity (e.g., Hirth and Kohlstedt 2004; Freed et al. 2017) and lateral variation of mantle viscosity (e.g., Dixon et al. 2004; Li et al. 2017) may also contribute to the observed surface deformation and complex the deformation pattern in detail (e.g., the gradients and localized features of surface deformation). Even though, our simple forward viscoelastic models are able to provide sufficient explanations on both the horizontal and vertical velocities (i.e., a few mm/year of model misfit, Fig. 2). Further studies, considering complex geological structures, might better fit the observed surface deformation and quantify the slip deficits and hence the seismic potentials along both megathrust and back-arc faults.

The interseismic stresses relaxed by the viscoelastic mantle propagate broadly across the continental faults and may trigger fault creeping of these preexisting weak zones. Our models show that the megathrust locking depth plays a relatively small role on the activation of the back-arc fault (Fig. 3 and 4b). In contrast, weak mantle has a strong influence on the activation of the back-arc fault, i.e., lower viscosity of the mantle results more active of the back-arc fault with the same frictional strength of the back-arc fault (Fig. 4a). Therefore, the activation of the continental fault on surface could potentially be an indicator of the mantle strength at depth. Lateral variation of the activation of the large-scale continental fault (such as the back-arc fault in South America) along the fault-strike direction may thus imply the lateral variation of the mantle strength, relating to the snapshots of long-term plate tectonic revolution (e.g., Chen et al. 2019). Nevertheless, in addition to the factors investigated in this study, some other geodynamic processes (e.g., the long-term mantle convection and the gravitational potential of the high-elevation Central Andes comparing to the low-elevation eastern basin) and even seasonal hydrological loading might also facilitate the activation of the back-arc fault and require future studies.

Our results indicate that the back-arc fault is remarkably weak ($\mu' < 0.1$) to be activated during the interseismic period (Fig. 4c and S4). This value is lower than the values (> 0.2) typically measured by sliding experiments in laboratory conditions (e.g., Di Toro et al. 2004). However, at the mature faults in nature, μ' is likely to be low with hydrostatic pore fluid pressure, supported by heat flow measurements (e.g., Gao and Wang, 2014), geodynamic/force-

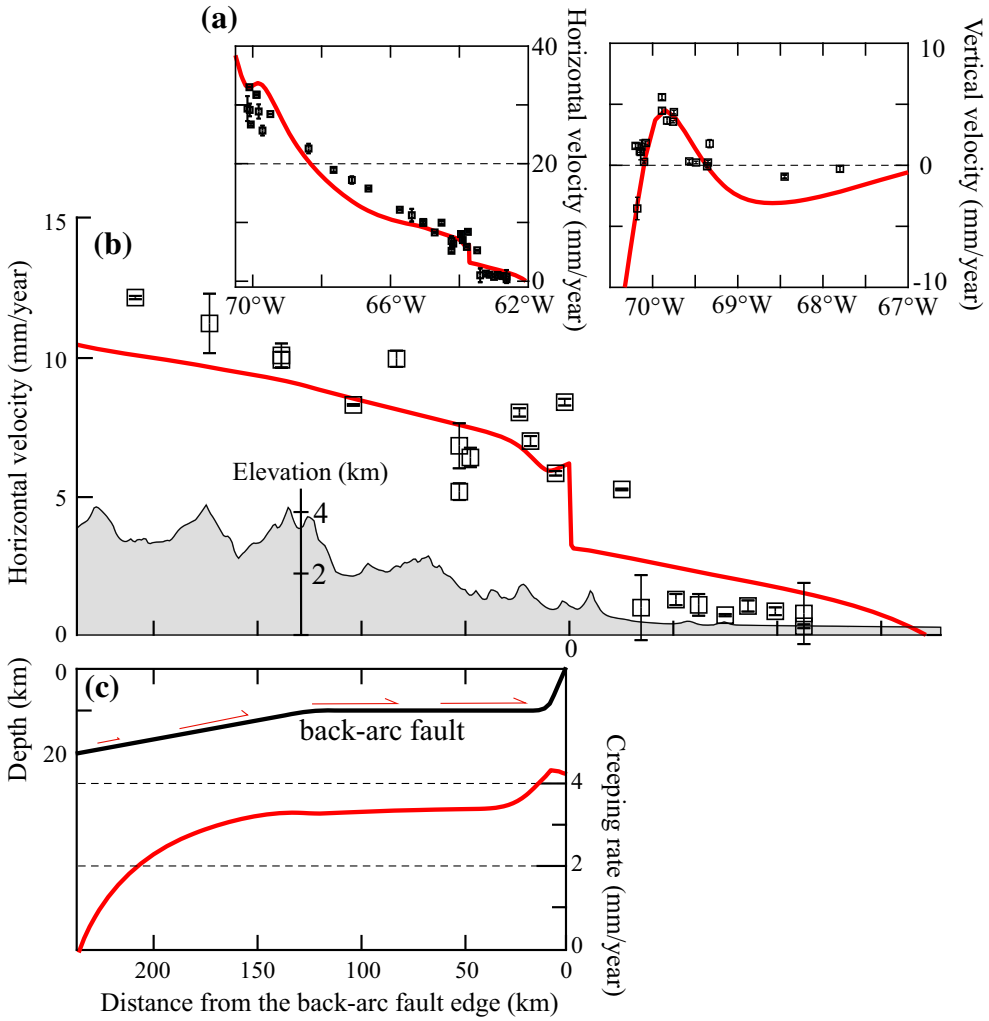

Figure 6
The performance of our optimal viscoelastic mechanical model. The subduction locking depth, the continental mantle viscosity, and μ' of the back-arc fault are 40 km, 3×10^{19} Pa s, and 0.001, respectively. **a** Overall model fitting of GPS-derived horizontal and vertical velocities. **b** Comparison of modeled deformation rates and topographic profile (gray curve) near the back-arc fault. **c** The geometry and simulated creeping rate of the back-arc fault

balance reasonings (e.g., Lamb 2006), and earthquake triggering along continental faults (Li et al. 2014). Readers interested in the topic of fault strength are referred to some recent publications (Brodsky et al. 2019; Dal et al. 2019; Li et al. 2018a). With a weak back-arc fault, our mechanical models reproduce the observed SVG and improve the fitting of the horizontal (Fig. 5a) and hence all (Fig. 5c) GPS-derived velocities. Based on these results, we propose our optimal mechanical model, which predicts the modeled SVG comparable to the GPS-derived surface velocities (Fig. 6a, b) and also predicts that the back-arc fault is largely creeping at $\sim$ 3 mm/year (Fig. 6c). Previous studies indicate that the fold-and-thrust belt in the back-arc is shortening at around the rate of 10 mm/year over the past 25 M year (Sheffels 1990; Schmitz 1994; Brooks et al. 2011; Oncken et al. 2012). Therefore, the back-arc fault may creep mostly aseismically but still accumulate a certain portion of slip deficit ($\sim$ 7 mm/year) during the interseismic period of large subduction zone earthquakes, which would be released eventually in

earthquakes with a longer period of recurrence than that of the subduction earthquakes. In Central Andes, the nature of weakness zones in the lithosphere in the back-arc seems play an important role on the distribution of the present-day interseismic deformation that surface velocities do not decay gently into the flat region in the hinterland but sharply to $\sim$ 0 mm/year at the edge of the Andes Mountain (Fig. 6a). Therefore, this kind of crustal fault may facilitate the localized strain accumulation near the crustal faults over subduction earthquake cycles (e.g., Luo and Liu 2009) and strain partitioning among crustal blocks (e.g., Bourne et al. 1998) across the geological time scales (e.g., Oncken et al. 2012).

6. Conclusion

1. There is an inherent ambiguity of constraining continental mantle viscosity and locking depth with the interseismic horizontal deformation rates, which could be diagnosed by additionally using the vertical rates.
2. The major back-arc fault in Central Andes is remarkably weak in terms of frictional fault strength (< 0.1) and its present-day motion is mainly driven by interseismic viscoelastic relaxation of the continental mantle.
3. The back-arc fault is inferred to creep largely at $\sim$ 3 mm/year, accumulate slip deficit at $\sim$ 7 mm/year, and shorten the continental plate. This structure has the potential of producing large earthquakes as evidenced by paleoseismology studies.

Acknowledgements

Horizontal GPS velocities used in this work are published by the previous study and the reference is provided in the paper. Vertical GPS velocities are retrieved from the daily time series from Nevada Geodetic Laboratory (http://geodesy.unr.edu/index.php; Blewitt et al. 2018) and provided in the supporting information. Fuqiang Shi was supported by the China Scholarship Council (201604190009) for a visit at German Research Centre for Geosciences (GFZ). Shaoyang Li is a JSPS International Research Fellow and was supported by the visiting program of Earthquake Research Institute, the University of Tokyo. Marcos Moreno acknowledges support from the Chilean National Fund for Development of Science and Technology (FONDECYT) Grants 1181479, the Millennium Nucleus The Seismic Cycle Along Subduction Zones Grant NC160025, and Research Center for Integrated Disaster Risk Management (CIGIDEN), CONICYT/FONDAP 15110017. We thank Mian Liu, Kelin Wang for insightful discussions and Jun'ichi Fukuda for an internal review. We thank the Editor Yuning Fu for handling our paper and two anonymous reviewer for constructive comments. Some of the figures in this paper were created with GMT software (Wessel and Smith 1998).

Author contributions SL and MM conceived the work; SF performed all the numerical simulations; SF and SL prepared the figures; SL analysized the vertical GPS data; SL wrote the paper with comments from MM.

References

Aagaard, B. T., Knepley, M. G., & Williams, C. A. (2013). A domain decomposition approach to implementing fault slip in finite-element models of quasi-static and dynamic crustal deformation. *Journal of Geophysical Research: Solid Earth, 118*(6), 3059–3079.

Allmendinger, R. W., Jordan, T. E., Kay, S. M., & Isacks, B. L. (1997). The evolution of the Altiplano-Puna plateau of the Central Andes. *Annual Review of Earth and Planetary Sciences, 25*(1), 139–174.

Bevis, M., Kendrick, E., Smalley, R., Brooks, B., Allmendinger, R., & Isacks, B. (2001). On the strength of interplate coupling and the rate of back arc convergence in the central Andes: an analysis of the interseismic velocity field. *Geochemistry, Geophysics, Geosystems*, *2*(11).

Blewitt, G., Hammond, W. C., & Kreemer, C. (2018). Harnessing the GPS data explosion for interdisciplinary science. *Eos*, *99*.

Bourne, S. J., England, P. C., & Parsons, B. (1998). The motion of crustal blocks driven by flow of the lower lithosphere and implications for slip rates of continental strike-slip faults. *Nature, 391*(6668), 655.

Brodsky, E. E., Mori, J. J., Anderson, L., Chester, F. M., Conin, M., Dunham, E. M., et al. (2019). The state of stress on the fault

before, during, and after a major earthquake. *Annual Review of Earth and Planetary Sciences, 48,* 2020.

Brooks, B. A., Bevis, M., Smalley Jr, R., Kendrick, E., Manceda, R., Lauría, E., Maturana, R., & Araujo, M. (2003). Crustal motion in the Southern Andes (26°–36° S): Do the Andes behave like a microplate? *Geochemistry, Geophysics, Geosystems*, *4*(10).

Brooks, B. A., Bevis, M., Whipple, K., Arrowsmith, J. R., Foster, J., Zapata, T., et al. (2011). Orogenic-wedge deformation and potential for great earthquakes in the central Andean backarc. *Nature Geoscience, 4*(6), 380.

Burgette, R. J., Weldon, R. J., & Schmidt, D. A. (2009). Interseismic uplift rates for western Oregon and along-strike variation in locking on the Cascadia subduction zone. *Journal of Geophysical Research: Solid Earth*. https://doi.org/10.1029/2008JB005679.

Chen, Y. W., Wu, J., & Suppe, J. (2019). Southward propagation of Nazca subduction along the Andes. *Nature, 565*(7740), 441.

Chlieh, M., Perfettini, H., Tavera, H., Avouac, J. P., Remy, D., Nocquet, J. M., Rolandone, F., Bondoux, F., Gabalda, G.. & Bonvalot, S. (2011). Interseismic coupling and seismic potential along the Central Andes subduction zone. *Journal of Geophysical Research: Solid Earth*, *116*(B12).

Cohen, S. C. (1984). Postseismic deformation due to subcrustal viscoelastic relaxation following dip-slip earthquakes. *Journal of Geophysical Research: Solid Earth, 89*(B6), 4538–4544.

Comte, D., & Pardo, M. (1991). Reappraisal of great historical earthquakes in the northern Chile and southern Peru seismic gaps. *Natural Hazards, 4*(1), 23–44.

Comte, D., Pardo, M., Dorbath, L., Dorbath, C., Haessler, H., Rivera, L., et al. (1994). Determination of seismogenic interplate contact zone and crustal seismicity around Antofagasta, northern Chile using local data. *Geophysical Journal International, 116*(3), 553–561.

Dal, L. Z., Gerya, T., & Avouac, J. P. (2019). Bimodal seismicity in the Himalaya controlled by fault friction and geometry. *Nature Communications, 10*(1), 48.

Di Toro, G., Goldsby, D. L., & Tullis, T. E. (2004). Friction falls towards zero in quartz rock as slip velocity approaches seismic rates. *Nature, 427*(6973), 436.

Dixon, J. E., Dixon, T. H., Bell, D. R., & Malservisi, R. (2004). Lateral variation in upper mantle viscosity: role of water. *Earth and Planetary Science Letters, 222*(2), 451–467.

Freed, A. M., Hashima, A., Becker, T. W., Okaya, D. A., Sato, H., & Hatanaka, Y. (2017). Resolving depth-dependent subduction zone viscosity and afterslip from postseismic displacements following the 2011 Tohoku-oki, Japan earthquake. *Earth and Planetary Science Letters, 459*, 279–290.

Gao, X., & Wang, K. (2014). Strength of stick-slip and creeping subduction megathrusts from heat flow observations. *Science, 345*(6200), 1038–1041.

Hirth, G., & Kohlstedt, D. (2004). Rheology of the upper mantle and the mantle wedge: a view from the experimentalists. *Inside the subduction Factory, 138,* 83–105.

Hyndman, R. D. (2017). Lower-crustal flow and detachment in the North American Cordillera: a consequence of Cordillera-wide high temperatures. *Geophysical Journal International, 209*(3), 1779–1799.

Isacks, B. L. (1988). Uplift of the central Andean plateau and bending of the Bolivian orocline. *Journal of Geophysical Research: Solid Earth, 93*(B4), 3211–3231.

Jaeger, J. C., & Cook, N. G. W. (1979). *Fundamentals of rock mechanics* (p. 585). London: Chapman & Hall.

Kendrick, E., Bevis, M., Smalley Jr, R., & Brooks, B. (2001). An integrated crustal velocity field for the central Andes. *Geochemistry, Geophysics, Geosystems*, *2*(11).

Lamb, S. (2006). Shear stresses on megathrusts: Implications for mountain building behind subduction zones. *Journal of Geophysical Research*. https://doi.org/10.1029/2005JB003916.

Li, S., Barnhart, W. D., & Moreno, M. (2018a). Geometrical and Frictional Effects on Incomplete Rupture and Shallow Slip Deficit in Ramp-Flat Structures. *Geophysical Research Letters, 45*(17), 8949–8957.

Li, S., Moreno, M., Bedford, J., Rosenau, M., Heidbach, O., Melnick, D., et al. (2017). Postseismic uplift of the Andes following the 2010 Maule earthquake: implications for mantle rheology. *Geophysical Research Letters, 44*(4), 1768–1776.

Li, S., Moreno, M., Bedford, J., Rosenau, M., & Oncken, O. (2015). Revisiting viscoelastic effects on interseismic deformation and locking degree: a case study of the Peru-North Chile subduction zone. *Journal of Geophysical Research: Solid Earth, 120*(6), 4522–4538.

Li, S., Moreno, M., Rosenau, M., Melnick, D., & Oncken, O. (2014). Splay fault triggering by great subduction earthquakes inferred from finite element models. *Geophysical Research Letters, 41*(2), 385–391.

Li, S., Wang, K., Wang, Y., Jiang, Y., & Dosso, S. E. (2018b). Geodetically inferred locking state of the Cascadia megathrust based on a viscoelastic Earth model. *Journal of Geophysical Research: Solid Earth, 123*(9), 8056–8072.

Loveless, J. P., & Meade, B. J. (2010). Geodetic imaging of plate motions, slip rates, and partitioning of deformation in Japan. *Journal of Geophysical Research: Solid Earth*, *115*(B2).

Luo, G., & Liu, M. (2009). How does trench coupling lead to mountain building in the Subandes? A viscoelastoplastic finite element model. *Journal of Geophysical Research: Solid Earth*, *114*(B3).

Matsu'Ura, M., & Sato, T. (1989). A dislocation model for the earthquake cycle at convergent plate boundaries. *Geophysical Journal International, 96*(1), 23–32.

McCaffrey, R., Long, M. D., Goldfinger, C., Zwick, P. C., Nabelek, J. L., Johnson, C. K., et al. (2000a). Rotation and plate locking at the southern Cascadia subduction zone. *Geophysical Research Letters, 27*(19), 3117–3120.

McCaffrey, R., Zwick, P. C., Bock, Y., Prawirodirdjo, L., Genrich, J. F., Stevens, C. W., et al. (2000b). Strain partitioning during oblique plate convergence in northern Sumatra: geodetic and seismologic constraints and numerical modeling. *Journal of Geophysical Research: Solid Earth, 105*(B12), 28363–28376.

Moretti, I., Baby, P., Mendez, E., & Zubieta, D. (1996). Hydrocarbon generation in relation to thrusting in the Sub Andean zone from 18 to 22 degrees S, Bolivia. *Petroleum Geoscience, 2*(1), 17–28.

Oncken, O., Boutelier, D., Dresen, G., & Schemmann, K. (2012). Strain accumulation controls failure of a plate boundary zone: Linking deformation of the Central Andes and lithosphere mechanics. *Geochemistry, Geophysics, Geosystems*, *13*(12).

Pope, D. C., & Willett, S. D. (1998). Thermal-mechanical model for crustal thickening in the central Andes driven by ablative subduction. *Geology, 26*(6), 511–514.

Savage, J. C. (1983). A dislocation model of strain accumulation and release at a subduction zone. *Journal of Geophysical Research: Solid Earth, 88*(B6), 4984–4996.

Schmitz, M. (1994). A balanced model of the southern Central Andes. *Tectonics, 13*(2), 484–492.

Sheffels, B. M. (1990). Lower bound on the amount of crustal shortening, in the central Bolivian Andes. *Geology, 18*(9), 812–815.

Sun, T., Wang, K., & He, J. (2018). Crustal deformation following great subduction earthquakes controlled by earthquake size and mantle rheology. *Journal of Geophysical Research: Solid Earth, 123*(6), 5323–5345.

Uba, C. E., Kley, J., Strecker, M. R., & Schmitt, A. K. (2009). Unsteady evolution of the Bolivian Subandean thrust belt: The role of enhanced erosion and clastic wedge progradation. *Earth and Planetary Science Letters, 281*(3–4), 134–146.

Wallace, L. M., Beavan, J., McCaffrey, R., & Darby, D. (2004). Subduction zone coupling and tectonic block rotations in the North Island, New Zealand. *Journal of Geophysical Research: Solid Earth*, *109*(B12).

Wang, K., Hu, Y., & He, J. (2012). Deformation cycles of subduction earthquakes in a viscoelastic Earth. *Nature, 484*(7394), 327.

Wang, K., Wells, R., Mazzotti, S., Hyndman, R. D., & Sagiya, T. (2003). A revised dislocation model of interseismic deformation of the Cascadia subduction zone. *Journal of Geophysical Research: Solid Earth*, *108*(B1).

Weiss, J. R., Brooks, B. A., Foster, J. H., Bevis, M., Echalar, A., Caccamise, D., et al. (2016). Isolating active orogenic wedge deformation in the southern Subandes of Bolivia. *Journal of Geophysical Research: Solid Earth, 121*(8), 6192–6218.

Wessel, P., & Smith, W. H. (1998). New, improved version of Generic Mapping Tools released. *Eos, Transactions American Geophysical Union, 79*(47), 579.

(Received June 15, 2019, revised December 4, 2019, accepted December 19, 2019)